

# OH Maser Sources in W49N: Probing Magnetic Field and Differential Anisotropic Scattering with Zeeman pairs using the VLBA

Avinash A. Deshpande<sup>1,2</sup>, W. M. Goss<sup>3</sup> and J. E. Mendoza-Torres<sup>4</sup>

## ABSTRACT

Our analysis of a VLBA 12-hour synthesis observation of the OH masers in a well-known star-forming region W49N has yielded valuable data that enables us to probe distributions of magnetic fields in both the maser columns and the intervening interstellar medium (ISM). The data consisting of detailed high angular-resolution images (with beam-width  $\sim 20$  milli-arc-seconds) of several dozen OH maser sources or *spots*, at 1612, 1665 and 1667 MHz, reveal anisotropic scatter broadening, with typical sizes of a few tens of milli-arc-seconds and axial ratios between 1.5 to 3. Such anisotropies have been reported earlier by Desai, Gwinn & Diamond (1994) and interpreted as induced by the local magnetic field parallel to the Galactic plane. However, we find a) the apparent angular sizes on the average a factor of about 2.5 less than those reported by Desai et al. (1994), indicating significantly less scattering than inferred earlier, and b) a significant deviation in the average orientation of the scatter-broadened images (by  $\sim 10$  degrees) from that implied by the magnetic field in the Galactic plane. More intriguingly, for a few Zeeman pairs in our set, significant differences (up to  $6\sigma$ ) are apparent in the scatter broadened images for the two hands of circular polarization, even when apparent velocity separation is less than  $0.1 \text{ km s}^{-1}$ . This may possibly be the first example of a Faraday rotation contribution to the diffractive effects in the ISM. Using the Zeeman pairs, we also study the distribution of magnetic field in the W49N complex, finding no significant trend in the spatial structure function. In this paper, we present the details of our observations and analysis leading to these findings, discuss implications of our results for the intervening anisotropic

---

<sup>1</sup>Raman Research Institute, Sadashivanagar, Bangalore, 560080 India; desh@rri.res.in

<sup>2</sup>University of Tasmania, Private Bag 21, Hobart 7001, TAS, Australia

<sup>3</sup>National Radio Astronomy Observatory, P.O. Box O, Socorro, NM 87801 USA; mgoss@aoc.nrao.edu

<sup>4</sup>Instituto Nacional de Astrofísica Óptica y Electrónica, Tonantzintla, Puebla, 72840, México; mend@inaoep.mx

magneto-ionic medium, and suggest the possible implications for the structure of magnetic fields within this star-forming region.

*Subject headings:* masers — ISM: molecules — magnetic fields — individual (W49N) — radio lines: ISM — structure function

## 1. Introduction

W49N is a well-known and extensively-studied massive star-forming complex in the Milky Way. The OH and H<sub>2</sub>O masers in this region represent some of the most luminous such sources in our Galaxy. The W49N complex, in the Galactic direction  $(\ell, b) = (43.17^\circ, 0.01^\circ)$ , is located on the far-side of the Solar circle. Its large distance ( $\sim 11.4$  kpc; Gwinn et al. 1992) and low Galactic latitude together make this object attractive for studying various propagation effects due to the intervening medium. The interstellar scattering in this case is comparable to that in the Vela direction (Gwinn et al. 1993), but the Vela pulsar is at a much smaller distance ( $\leq 1$  kpc).

In our efforts to study intrinsic short timescale variability in W3OH (Ramachandran et al. 2006; also Laskar et al. 2012) we were able to estimate and remove possible variability due to interstellar scintillation using the fact that the decorrelation bandwidth is larger than the measured line widths. Such velocity-resolved analysis of W3OH data has suggested intrinsic variability on 15-20 minute time scale (Ramachandran et al. 2006), whereas W49N data show variations on timescales of 1 hour or longer (Goss et al. 2007: talk at IAUS 242, Alice Springs). The timescales of apparent intrinsic variability, combined with light-travel-time-argument, suggest spatial scales for the maser columns to be a few AU for the OH sources in W3OH complex (Ramachandran et al. 2006). The reliability of similar estimation in the case of W49N sources depends, however, on how well the contamination due to interstellar scintillation can be separated from the observed variability, particularly when the scintillation decorrelation bandwidth may not be much wider than the line widths. In fact, for the purpose of this variability study, W49N was included in our VLBA observations as a *comparison* source, where scattering effects are expected to dominate in the apparent relative variability of different spectral features due to the interstellar scintillations (with decorrelation bandwidth comparable or smaller than the line widths). The subsequent analysis of the data on this source has turned out to be far more fruitful than our initial expectations, revealing several interesting aspects that we describe and discuss in this paper.

Measurements of Galactic magnetic fields and of their distribution over a range of scales continue to be great interest, given their important role in the physical processes in the

interstellar medium. Magnetic fields present in molecular clouds become directly measurable through the Zeeman splitting of the narrow spectral lines associated with several species (e.g., Sarma et al. 2000, and references therein), and those threading across the intervening ionized medium manifest themselves through Faraday rotation and anisotropic scattering. While both the Zeeman splitting of nonmaser lines and the Faraday rotation depend on the line-of-sight component of the magnetic field, the anisotropy in scattering relates to the field component in the plane of the sky. However, in cases where the Zeeman splitting exceeds the individual line widths (as is often the case for narrow maser lines such as OH), the line separation is then dependent on the *total* field strength (Heiles et al. 1993) and not just the component along the line of sight.

In an earlier study of OH maser sources in W49N, Desai, Gwinn & Diamond (1994; hereafter DGD94) have found significant anisotropic scattering, attributable to electron-density irregularities that are preferentially elongated in the Galactic plane, due to a magnetic field parallel to the plane.

Our VLBA observations, and the resultant images of several dozen maser spots (including a few dozen Zeeman pairs), provide significantly improved statistics to investigate in greater detail the anisotropic scattering, as well as to probe the distribution of magnetic fields within the W49N complex. Some of our findings are in good qualitative agreement with those of DGD94; they however differ quantitatively from their estimates of scatter-broadened source sizes as well as the mean source position angle (hereafter SPA) characterizing the apparent shapes of the maser spots. These observations provide a rare opportunity to look for another imprint of the magnetic fields in the scattering medium, namely, possible differential diffraction experienced by opposite circular polarization components of propagating electromagnetic waves. This expectation is based on the same refractive index differences for the two circulars that result in Faraday rotation of the position angle of the linear component of incident polarization.

Our data on 32 Zeeman pairs, providing estimates of magnetic field within the maser column, enables us to study the distribution and variation of the magnetic field in this star-forming complex.

In the following section, we describe briefly our observations and data which form the basis for the analysis and results discussed in the paper. Section 3 presents our general findings on the anisotropic scattering observed in the direction of the OH sources in W49N. The data suggesting significant differential anisotropic scattering, probed using Zeeman pairs, are described in section 4. The structure functions of the magnetic field local to the source, as well as the scattering parameters estimated for the ensemble, are presented in section 5. The implications of our results are discussed and summarized in the final section.

## 2. Our data

Our visibility data from 12+ hour synthesis observations with VLBA (BR107; 2005 July) were calibrated & processed in the standard way using AIPS. The data were self-calibrated; absolute coordinates are not available due to an absence of phase reference source observations. The spectral-line image cubes, obtained separately at 1612, 1665 & 1667 MHz, provided high angular-resolution images of the set of sources for each of the transitions, for each of the circular polarizations. The total imaged angular extent of about 8 arc-seconds corresponds to a transverse span of  $\sim 0.5$  pc at the distance of the source, although a majority of the sources are within the central 2 arc-second region. As a result of exclusion of the outer 2 antennas of the VLBA (St. Croix & Mauna Kea) from self-calibration, due to lack of visibility of the sources on those baselines in this imaging, the synthesized beam size across (RA,Dec) is  $20 \times 15$  mas. (the corresponding spatial resolution is about  $\sim 175$  AU at the distance of W49N). The lack of visibility on the longest baselines is consistent with, and is in fact due to, the apparent angular sizes of the maser sources in the range 20-40 mas. Each data set consisting of cleaned and restored images across 240 spectral channels spanning a  $22 \text{ km s}^{-1}$  velocity range, providing velocity resolution of  $\sim 0.1 \text{ km s}^{-1}$ , was used to identify discrete maser sources (avoiding cases with significant velocity gradients). For each of clearly identifiable discrete (or isolated) maser sources, best-fit estimates of the *deconvolved* source shape and size were obtained, in addition to the estimates of the mean location and velocity, along with estimates of the respective uncertainties. For these estimations, we have used a procedure in AIPS (JMFIT), which facilitates fitting of a 2-d Gaussian to a source image and returns the best-fit parameters, including errors. The shape and size together are parametrized in terms of major & minor axes and position angle associated with a model ellipse describing the cross-section of a 2-d Gaussian sampled at half-power points. Although the absolute position information is uncertain by an unknown amount, the relative positions of the sources at both 1665 & 1667 MHz are reliable within the estimation uncertainties, as same self-calibration applies to the data at these two frequencies. The resultant data on a total of 205 sources (194 of these at 1665 & 1667 MHz) were examined for positional proximity of left and right circular polarization (LCP and RCP, respectively) source pairs ( $\leq 10$  mas), and 32 Zeeman pairs were thus identified. Figure 1 shows the distribution of all discrete sources in the RA-Dec plane; the size of the symbol is proportional to the mean velocity associated with the observed OH line. The circles and stars denote the sources with RCP and LCP, respectively. Most of the sources are within an area extending from RA-Dec offset (in mas) of (-2000,-2000) to (+4000,+4000). The velocities (indicated crudely by the symbol size) on the average differ systematically between the two halves about the center of this area (roughly at RA-Dec offset of 1000,1000 mas). An overall correlation between the locations of the sources on the sky plane and their line-of-sight velocities, such as that

evident for the distribution in the Figure 1, is to be expected in system morphologies dictated by rotation and/or bipolar outflows that are commonly encountered in star-forming regions (see, for example, Shepherd and Churchwell 1996).

### 3. Anisotropic scattering: apparent source sizes and shapes

Scatter-broadened shapes and orientations of the maser spots provide valuable information on the nature of the scattering medium. Figure 2 displays the deconvolved sizes of the sources, giving the dimensions along the major and the minor axes of the respective best-fit ellipses. The elongations or the axial ratios (ratio of major to minor axis of the best-fit ellipse) for a majority of the sources are in the range 1.5 to 3, indicating significant anisotropic scattering, consistent with the finding of DGD94. However, we find the overall apparent sizes of the sources to be significantly smaller (by a factor of  $\geq 2$ ) than those reported by DGD94. Our size estimates are nonetheless consistent with the suitably scaled values of the scatter-broadening of H<sub>2</sub>O masers reported by Gwinn (1994), i.e. about 40 mas (200  $\mu$ as times  $[18/1.3]^2$ ). Interesting, DGD94 themselves mention about 45 mas as the expected amount of scatter broadening at 18 cm wavelength for the W49N sources. Possible reasons for what appears to be an overestimation of the sizes in DGD94 are entirely unclear at present. However, we note that the larger apparent angular sizes for the sources reported by DGD94 would necessarily imply significant loss of visibility on a larger fraction of the VLBA baselines, an effect which should be readily apparent.

One of the most important aspects discussed by DGD94 (also see references therein) is that the apparent image sizes/shapes are expected to be elongated orthogonal to the scattering irregularities due to anisotropic diffraction. The presence of a magnetic field would induce such anisotropy in the electron-density irregularities; then the implied field direction would be perpendicular to the resultant image position angle (i.e. SPA). Based on their limited sample, of the apparent image shapes for 27 spectral components from 6 of the OH maser sources in W49N, DGD94 suggested that the apparent anisotropy is induced by a magnetic field in and parallel to the Galactic plane.

In Figure 3, we present a distribution of our estimates of the SPAs for our significantly ( $\sim 30$  times) larger sample. Some random spread in SPA is apparent in both our and DGD94’s reported SPA values; such a spread ( $\sim 5$  degrees r.m.s.) is not unexpected, given the estimation uncertainties as well as possible differences in the scattering sampled by different lines of sight. However, we find that our SPA distribution has a significant offset from the SPA of  $\sim 117$  degrees, the expected SPA if the density irregularities are elongated parallel to the Galactic plane. Our sample gives a mean SPA of  $107 \pm 3$  degrees, implying

a significant mean deviation, of  $\sim 10$  degrees, in the orientation of the density irregularities from the Galactic plane. The DGD94 sample may have been too limited to make such an offset detectable. We discuss below possible reasons for this systematic offset. If the large-scale magnetic fields in the intervening region has a 10 degree orientation with respect to the Galactic plane, or if the Galactic warp (e.g., Burton 1988) is responsible for this offset, then the observed orientations for the scatter-broadened images would be consistent with a correspondingly revised expectation. However, W49N is located almost on the farther edge of the inner (Solar) circle of our Galaxy, at a Galactic longitude of about 43 degrees, and the effect of the warps is observed to be more pronounced in the outer regions of our Galaxy. In any case, a look at the magnetic field structure along the W49N direction would be instructive. Interestingly, the sight-line to W49N is through the well-known North Polar Spur (NPS) feature (distance to the NPS is about 250 pc). From the study, by Wolleben (2007) and others of the NPS, it is evident that significantly different magnetic field structure as well as enhanced scattering would be expected for the medium within 0.5 kpc of the Sun. We note that the field orientation in this region, corresponding to the NPS, might be at a large inclination, if not almost orthogonal, to the Galactic plane (see Wolleben 2007 for details). Also, given that the scattering medium closer to the observer is expected to make relatively higher contribution to the angular broadening (e.g., Gwinn et al. 1993, Deshpande and Ramachandran 1998), the above mentioned SPA deviation can be caused by the more local scattering in the NPS region, with density anisotropy at a possibly large angle with respect to the Galactic plane.

The scattering in the W49N direction is unlikely to be dominated by any single thin screen, but is contributed by the entire magneto-ionic medium distributed between the Sun and the source. Although a detailed modelling of the magneto-ionic medium incorporating the relative strengths and sense of anisotropic scattering, associated magnetic field strengths and orientations for the different regions along the sight-line is needed to assess the net effect, we have carried out a simple simulation of propagation through multiple screens in order to examine the basic situation. For each screen, a random column-density distribution of free electrons, following a power-law spatial spectrum (with Kolmogorov index  $-11/3$ ) was used to simulate a 2-d scattering screen with a mild (1.6) anisotropy across a transverse extent of a few times the Fresnel scale ( $a_F = \sqrt{\lambda D}$ , where  $\lambda$  is the observing wavelength and  $D$  is the distance to the source). The orientation of the mean anisotropy in the screen nearest the observer was chosen to be orthogonal to those in the rest of the screens, consistent with the possible elongation of density irregularities in NPS region with respect to that parallel to the Galactic plane. A model with incoherent combination of the scatter broadening from such screens cannot produce a resultant image with an in-between orientation or SPA, for

example, with 10 deg offset as mentioned above, but would instead dilute the aspect ratio.<sup>1</sup> Hence, the spatial scales of relevant density irregularity in the phase-screens are likely to be very much larger than the sizes estimated based on the observed angular broadening, assuming a single thin screen. The relevant spatial scale of density irregularity should be adequately large, so that emerging wavefront (or field) retains memory of and is the result of the *coherent* combination of phase structure contributed by all sub-screens along the sight-line. The relevant phase structure should necessarily contain higher order variations and/or a finite random spread in orientations of phase curvatures.

#### 4. Differential Anisotropic Scattering: probe with Zeeman pairs

Thirty two Zeeman pairs can be identified from the large sample of sources using a positional-proximity criterion ( $\leq 10$  mas). Based on these Zeeman pairs we can probe a previously unobserved aspect of scattering caused by the magneto-ionic component of the interstellar medium. A magneto-ionic medium would, in principle, have differing refractive indices for signals corresponding to the two hands of circular polarization. Diffractive scintillation and scatter-broadened image shapes should therefore differ between the LCP and RCP due to any line-of-sight component of the magnetic field in the intervening medium. Hence scattering-dominated images of even a randomly polarized source might show circular polarization in unmatched parts of the images, if Faraday rotation is significant. Macquart & Melrose (2000) consider this possibility, but estimate the effect to be too small (circular fraction  $\sim 10^{-8}$ ) to be observable. Contrary to that expectation, the scatter-broadened images of some of the W49N OH maser sources seem to significantly differ in LCP and RCP, i.e. within a given Zeeman pair. For the remainder of the Zeeman pairs, the SPA differences are either small or within the respective uncertainties. Figure 4 shows the observed differences in the image shape parameters for a subset of our sample of Zeeman pairs. The subset includes only those cases for which a significant difference ( $\geq 6\sigma$ ) in image SPA is observed. Although there are only a few such Zeeman pairs, the SPA differences range between 6 to 30 degrees. Difference in the line velocities within most of these pairs is too small to account for the apparent differential scattering. Position differences are also within a few mas (i.e. much smaller compared to the scatter broadening), and are unlikely to contribute to the observed SPA differences. One such example of a significant SPA difference is shown in Figure 5.

---

<sup>1</sup> This situation has much in common with the polarization state resulting from combination of signals in two mutually orthogonal (say, linear) polarization states. A different orientation is possible only if the polarized components are at least partially mutually coherent, or else, the resulting net polarization would match that of the dominant of the two components, with a reduction in the degree of polarization.

To explore the issue further, we have made preliminary attempts to simulate signal propagation through a magneto-ionic medium with a mild anisotropy. Here a single, thin scattering screen was simulated, following the procedure outlined in an earlier section. For simplicity, a uniform magnetic field is assumed, so that the phase screens for the two circular polarizations are merely scaled versions of each other. The net circular polarization, if viewed with coarse resolution would be negligible, consistent with the conclusion of Macquart & Melrose (2000). However, when observed with adequately high angular resolution (e.g. 10 milli-arc-second), the simulations do reveal noticeable differential diffractive effects, hence differing shapes and sizes of scatter-broadened images for the two circular polarizations. The differential phase contribution due to the Faraday rotation should be significant, even if relatively small in comparison with the phase variation common to both polarizations. The data on rotation measures to several pulsars (Manchester et al. 2005; ATNF Pulsar Catalog<sup>2</sup>) close to the direction of W49N suggest that the expected Faraday rotation at 18 cm would correspond to about 30 radians of differential phase between the two circular polarization signals. In comparison, the phase structure function (Armstrong, Rickett & Spangler 1995) value at 1 AU scale (close to the Fresnel scale, given the distance to W49N and the wavelength of 18 cm) would suggest an rms phase fluctuation of the order of 300 radians, common to both polarizations. Hence, the differential phase contribution here can lead to noticeable differential scattering. Of course, more detailed and realistic simulations, i.e. with thick screens, are required to assess these issues in detail. However, the Faraday rotation contribution leading to differential anisotropic scattering for the two circular polarization signals remains a more natural explanation for the detected differences in source position angles. If true, the above would be the first such example of this effect in an astronomical context, as far as we are aware.

## 5. Spatial structure functions

The sight-lines to the two hundred or so sources spread across the W49N region potentially sample variations on a range of transverse scales within the region, as well as the intervening scattering medium. The estimated parameters for this set of scatter-broadened maser sources thus provide an excellent opportunity for probing the spatial scales associated with the variation in these parameters. However, since this sampling is rather non-uniform, we prefer to compute spatial structure functions using these data instead of trying to estimate the associated spatial power spectra. Although we treat each of the maser sources as a separate source, irrespective of their Zeeman pairing, we compute the structure functions

---

<sup>2</sup> <http://www.atnf.csiro.au/research/pulsar/psrcat>



separately for the pairs of sources with matching and opposite signs of circular polarization, along with the structure function for the entire source sample.

Given the limited signal-to-noise ratio in estimation of most of the parameters, the estimated structure functions will have corresponding noise bias. To assess the latter, we also computed the structure function contribution expected from uncertainties in the estimations of the relevant parameters. Figures 6, 7 and 8 show a few examples of the structure functions estimated in this manner, where the noise bias is relatively small. Specifically, in Figure 6 we present the structure function of the (line-of-sight) velocity associated with the sources. The clear linear trend in the log-log plot is consistent with the underlying velocity gradient across the region, manifesting the possible bipolar outflow morphology. Figure 7 shows the structure functions for the scatter-broadened size of the sources, in this case the minor axis associated with the elliptical source shape. Significant variations in the scattering property is apparent on an angular scale of about 200-300 mas. For an average distance to the scatterer of about half-way to the source (5.7 kpc), this angular scale would correspond to a spatial scale of 1000-1500 AU over which scatter broadening appears to change significantly.

The spatial structure function computed for the magnetic field using estimates available for the set of Zeeman pairs, as presented in Figure 8, shows no significant monotonic trend. This poor sampling of the structure function is largely due to the uneven and sparse sampling of the spatial scales that the available Zeeman pairs in this region offer. However, the scale on which the magnetic field appears to be decorrelated is about 150 mas (or 1500 AU spatial scale at the source distance). For 10 out of the 32 pairs, the Zeeman splitting is smaller than the line widths. Hence in these cases, the estimated magnetic field would correspond to only the line of sight component.

## 6. Summary

The OH maser sources in W49N show anisotropic scattering; the apparent scatter broadening is much less than reported earlier. The implied scintillation decorrelation bandwidth, corresponding to the observed sizes of the W49N sources ( $\geq 20$  mas), would be about 100 Hz (typical line widths are 2.5 kHz). This would correspond to a velocity width of 20 m/s, less than our velocity resolution (100 m/s). The sizes reported by DGD94 would have implied even narrower decorrelation bandwidths. Hence, we expect interstellar scintillations to be significantly quenched, reducing potentially contaminating contribution to any apparent intensity variability.

The position angles of the source images deviate significantly from the value expected if

scattering density irregularities were to be “stretched” due to magnetic field strictly aligned parallel to the Galactic plane, indicating significant scatter-broadening contribution from differently aligned density irregularities. This contribution may be associated with the North Polar Spur, within a distance of 0.5 kpc. Some of our data also reveal differential scattering during propagation of the two circular polarizations, likely caused by Faraday rotation. Through various aspects discussed above, the attractive, but yet unexplored, potential of the high-resolution maser observations for probing the intervening magneto-ionic medium is certainly evident.

The structure function analysis of the various parameters suggests spatial scales of a few thousand astronomical units over which the scattering properties in the intervening medium as well as the magnetic field in the maser region appear to be changing.

### **Acknowledgements:**

It is a pleasure to acknowledge the contributions from R. Ramachandran and Sarah Streb at different stages of the reported work. We thank Don Melrose and the anonymous referee for their valuable comments. AAD gratefully acknowledges fruitful discussions with Rajaram Nityananda, Simon Ellingsen and John Dickey. The National Radio Astronomy Observatory is a facility of the National Science Foundation operated under a cooperative agreement by Associated Universities, Inc.

*Facilities:* VLBA

### **REFERENCES**

- Armstrong, J. W., Rickett, B. J., & Spangler, S. R. 1995 ApJ, 443, 209
- Burton, W. B. 1988, *Galactic and extragalactic radio astronomy*, Berlin and New York, Springer-Verlag, 1988, p. 295-358
- Desai, K. M., Gwinn, C. R., & Diamond, P. J. 1994, Nature, 372, 754 (DGD94)
- Deshpande, A. A., & Ramachandran, R. 1998, MNRAS, 300, 577
- Gwinn, C. R., Moran, J. M., & Reid, M. J. 1992, ApJ, 393, 149
- Gwinn, C. R., Bartel, N., & Cordes, J. M. 1993, ApJ, 410, 673

Gwinn, C. R. 1994, *ApJ*, 429, 253

Heiles, C., Goodman, A. A., McKee, C.F., & Zweibel, E. G. 1993, In *Protostars and Planets III*, ed. E. H. Levy, J. I. Lunine (Tuscon: Univ. Ariz. Press), p. 279-326

Macquart, J.-P., & Melrose, D. B. 2000, *ApJ*, 545, 798

Manchester, R. N., Hobbs, G. B., Teoh, A., & Hobbs, M. 2005, *ApJ*, 129, 1993

Ramachandran, R., Deshpande, A. A., & Goss, W. M. 2006, *ApJ*, 653, 1314

Sarma, A. P., Troland, T. H., Roberts, D. A., & Crutcher, R. M. 2000, *ApJ*, 533, 271

Shepherd, D. S., & Churchwell, E. 1996, *ApJ*, 472, 225

Wolleben, M. 2007, *ApJ*, 664, 349

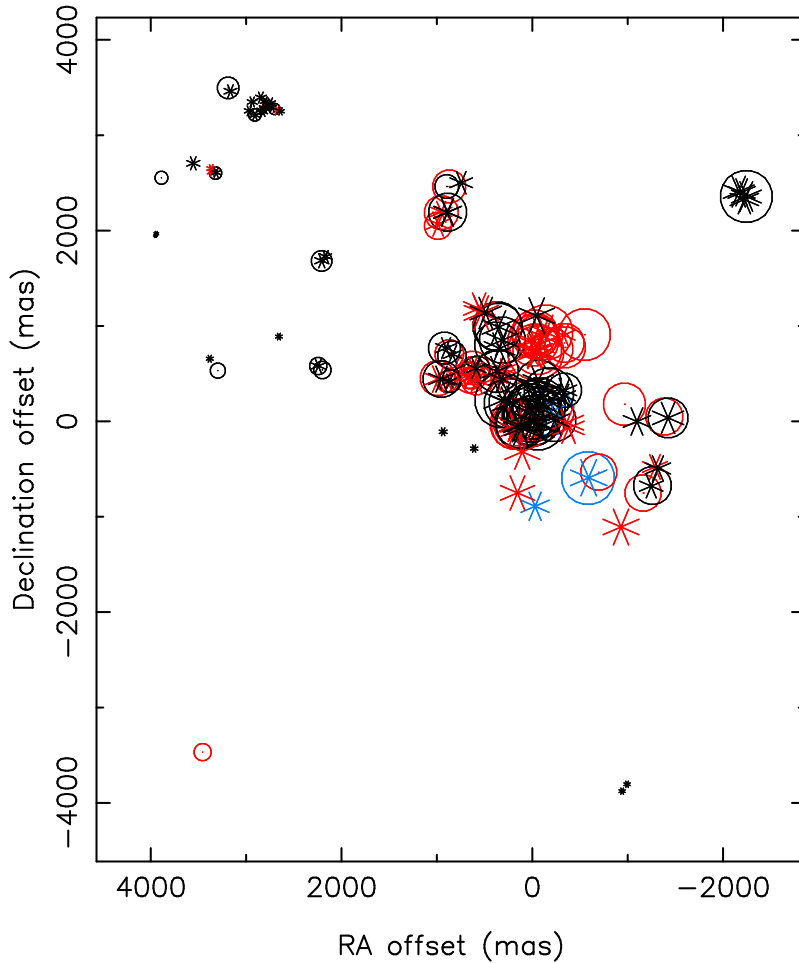


Fig. 1.— Observed distribution of W49N OH maser sources in RA-Dec. 2000 mas corresponds to 0.11 pc at the 11.4 kpc distance of W49N. The symbols in blue, red and black denote the sources at 1612, 1665 and 1667 MHz, respectively. The circles and stars refer to the Left and the Right hand circular polarization, respectively. The symbol sizes are scaled proportional to the velocity (which are in the range  $+2$  to  $+21$  km s $^{-1}$ ). The velocity-position correlation and an implied bipolar nature is apparent from the majority of the sources in the sample. (See the main text for details.)

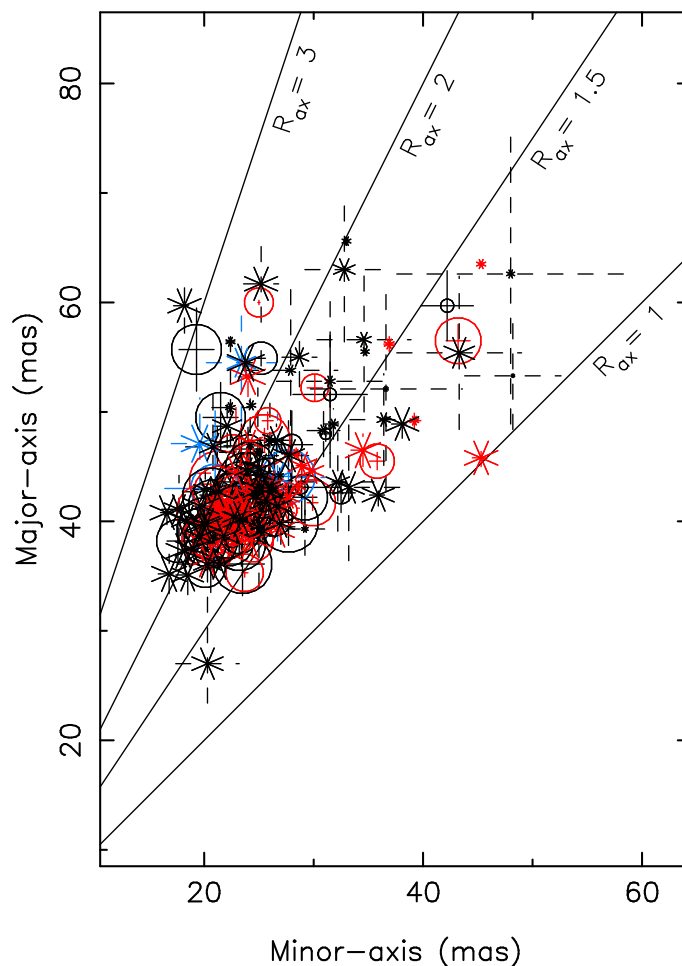


Fig. 2.— Scatter plot of the Major axis versus the Minor axis values estimated for the 205 spots, along with their  $1\sigma$  uncertainties indicated by the error bars. The correspondence of the symbols, including their colour and sizes, with the source parameters is same as that in the Figure 1. The four lines across the plot (from bottom to top) correspond to axial ratio,  $R_{ax}$ , of 1, 1.5, 2. and 3, respectively. A majority of the sources have axial ratios in the range 1.5 to 2.

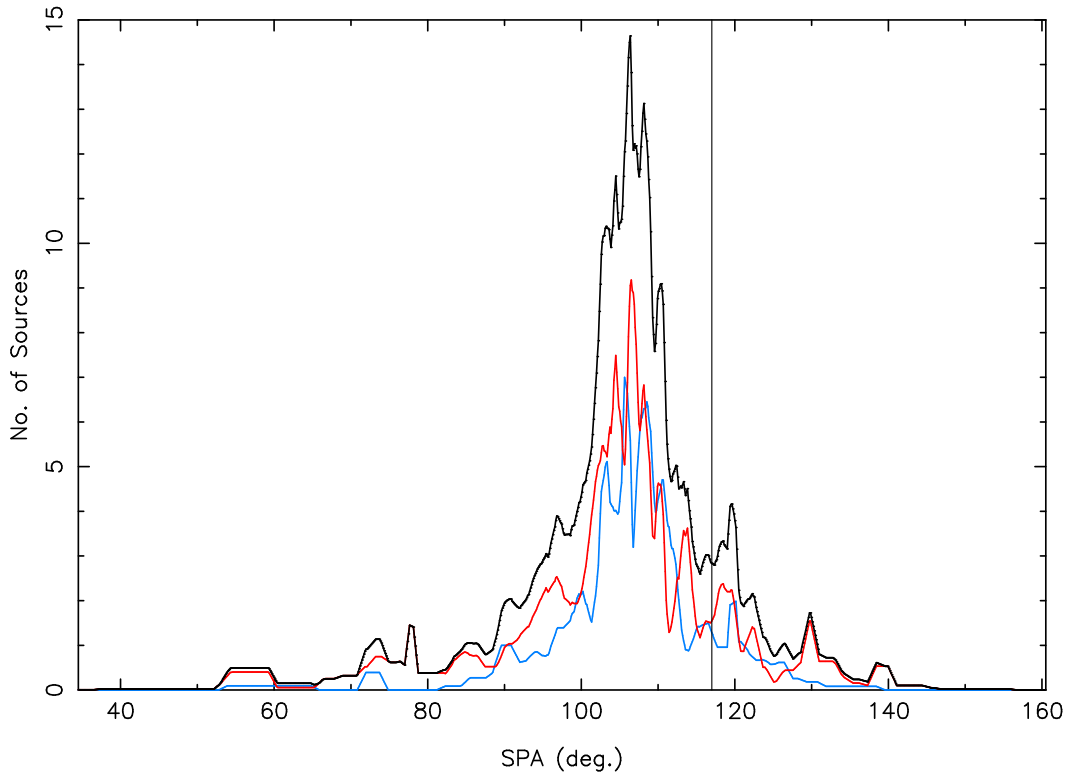


Fig. 3.— Distribution of the source position angles (SPAs) of the scatter-broadened images for our full set of OH maser sources in W49N is shown (black profile). The vertical line at 117 degrees, shown for reference, corresponds to an angle orthogonal to the Galactic plane. This is the value of SPA that would be expected from the anisotropic scattering due to electron density irregularities, if these are elongated parallel to the Galactic plane. The distributions of SPA shown here are after accounting for uncertainties in individual measurements (the blue and red profiles correspond to RCP and LCP, respectively). This distribution is used to estimate the mean SPA of the observed scatter-broadened images ( $107 \pm 3$  degrees).

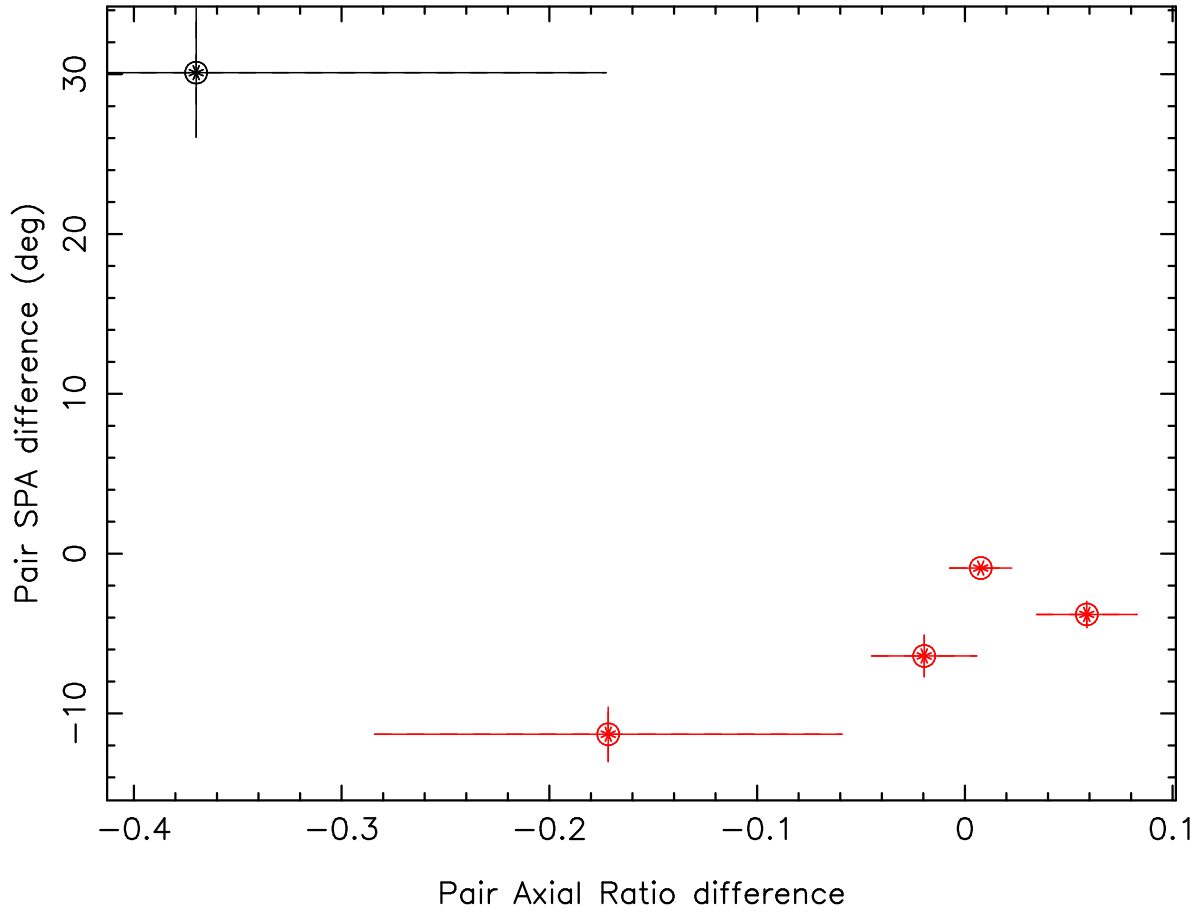


Fig. 4.— The SPA differences within Zeeman pairs versus the respective differences in axial ratios for the cases where significant SPA differences are apparent. The error bars indicate  $\pm 1\sigma$  uncertainties. Only one of these four sources is at 1667 MHz (in black), while the other three (in red) are at 1665 MHz. The axial ratios are consistent with equality of RCP and LCP

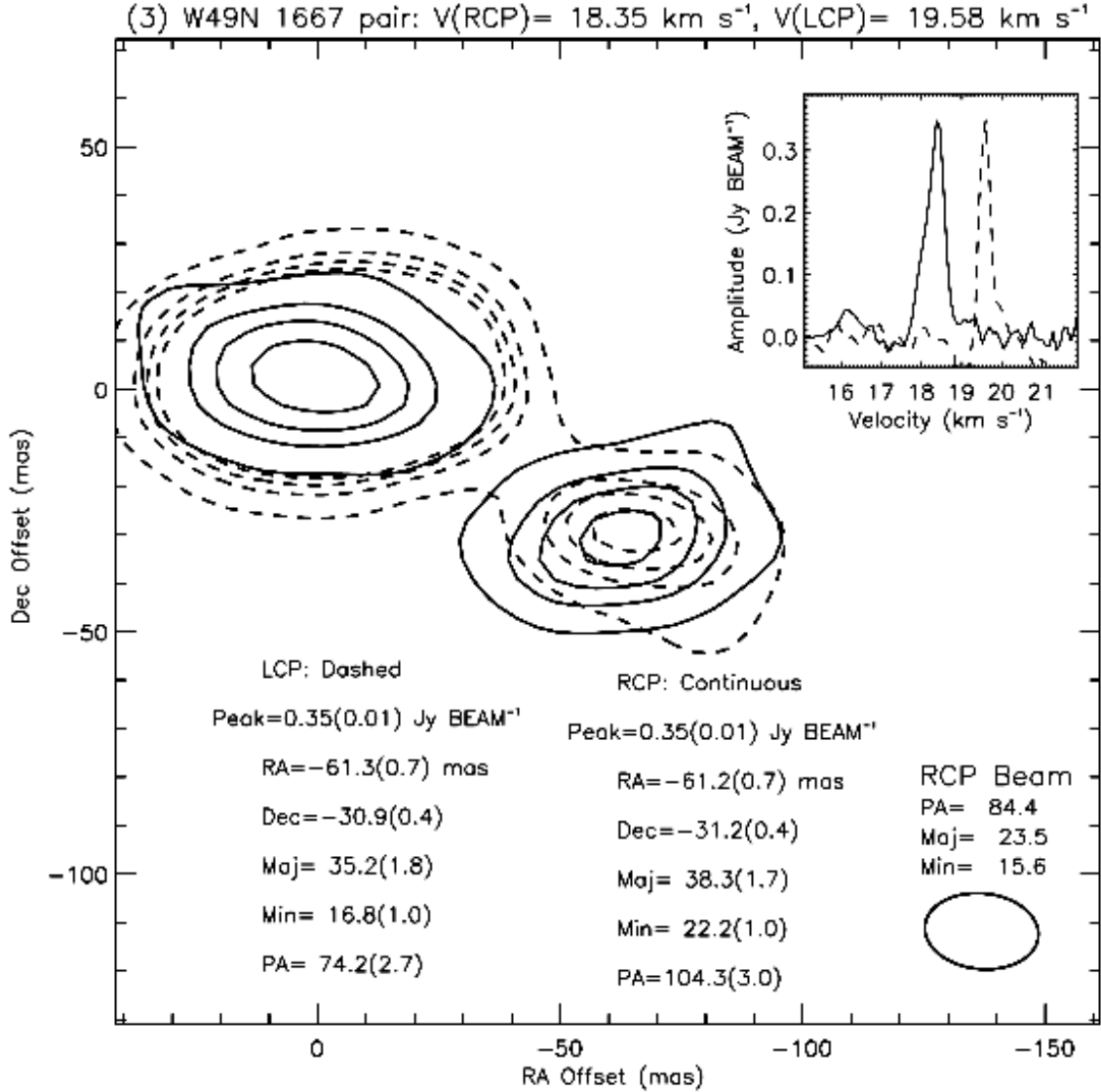


Fig. 5.— Apparent images are shown for the sources (at RA-DEC offsets -60 and -30 mas respectively) in both hands of circular polarization, i.e. for the Zeeman pair, where a significant difference (about 30 degrees) in the position angles of the scatter broadened shapes in the two circular polarization is evident. The associated line profiles are shown in the upper inset. The source at RA-DEC offsets of about 0,0, is also shown for comparison, where the image ellipses in the two circular polarizations have mutually consistent orientations.



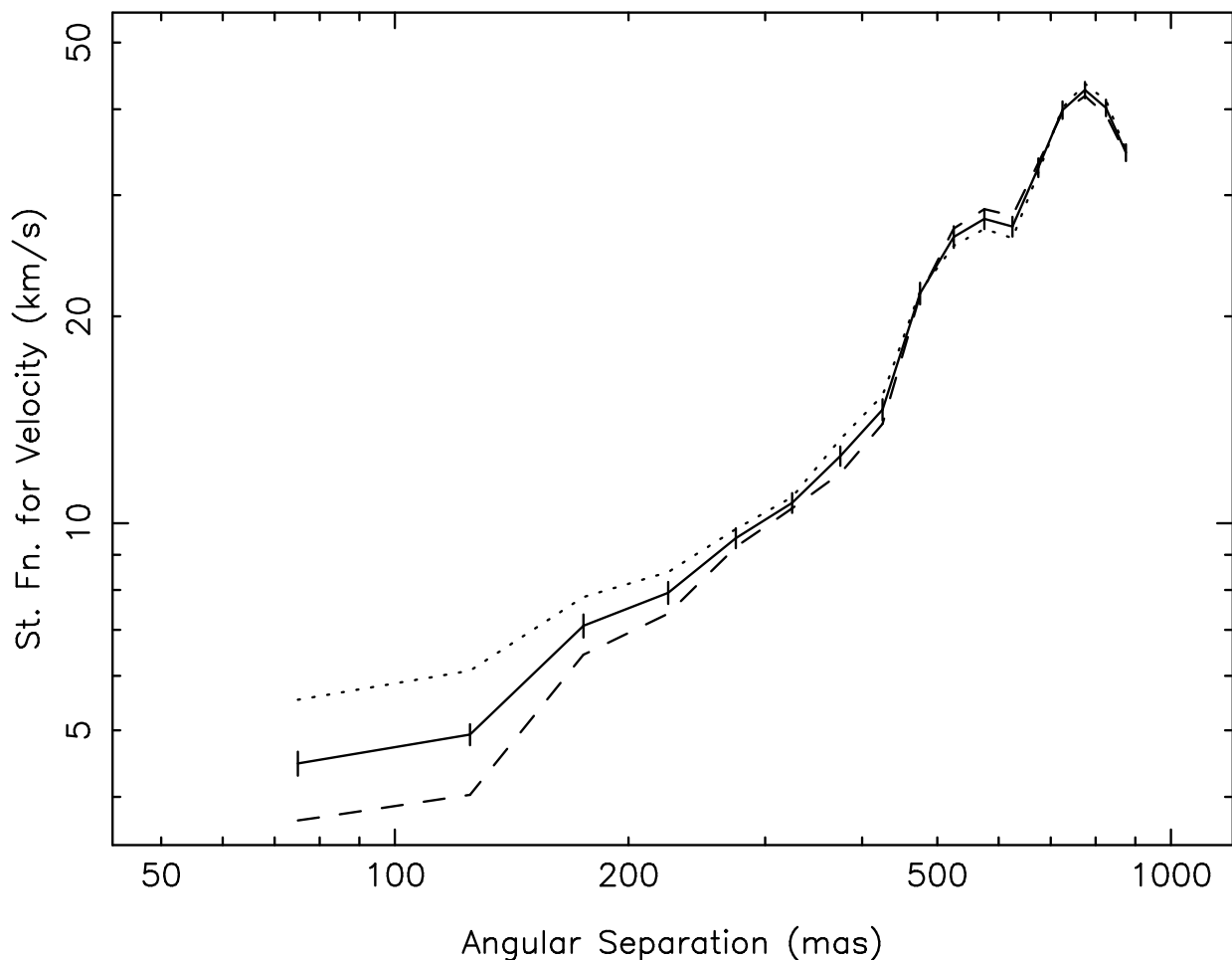


Fig. 6.— Spatial structure function of the line-of-sight velocity. The structure function values are in  $(\text{km s}^{-1})^2$ . The solid-line curve corresponds to the contribution from all source pairs, while the curves drawn with dashes and dots correspond to source pairs with matching and opposite circular polarization, respectively. The observed trend in the structure function is consistent with the velocity gradient across the source. Such position-velocity correlation is typical of a systematic velocity field, such as those found in bipolar outflows. The  $1\sigma$  error bars (shown only for the solid-line curve) include contributions from both the measurement and the statistical uncertainties in the estimates.

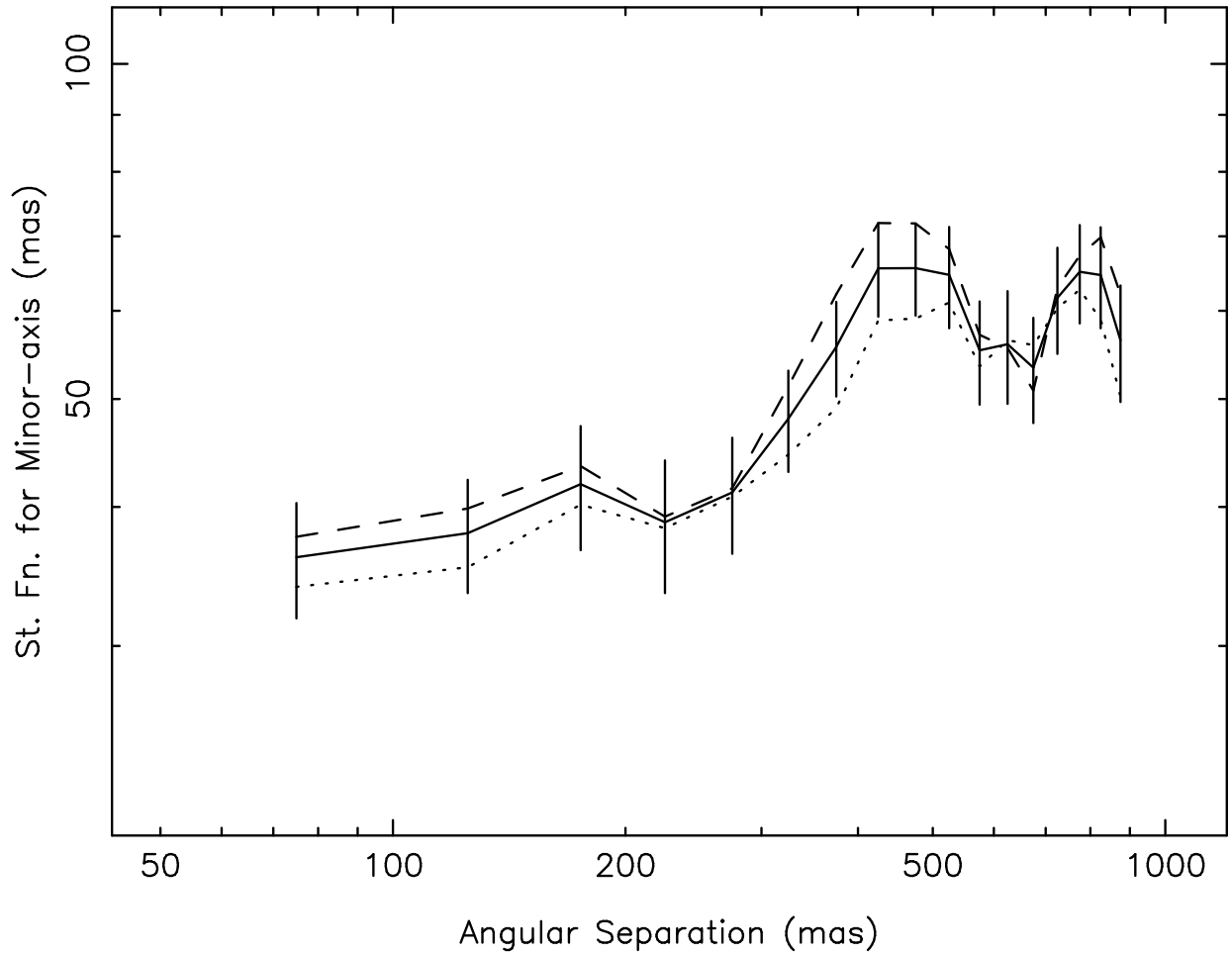


Fig. 7.— Similar to Figure 6, for the minor-axis size associated with the scatter-broadened images. The structure function is in units of  $(\text{mas})^2$ . The average trend in the above figure suggests that scattering properties have significant differences on angular scales larger than 200 mas.

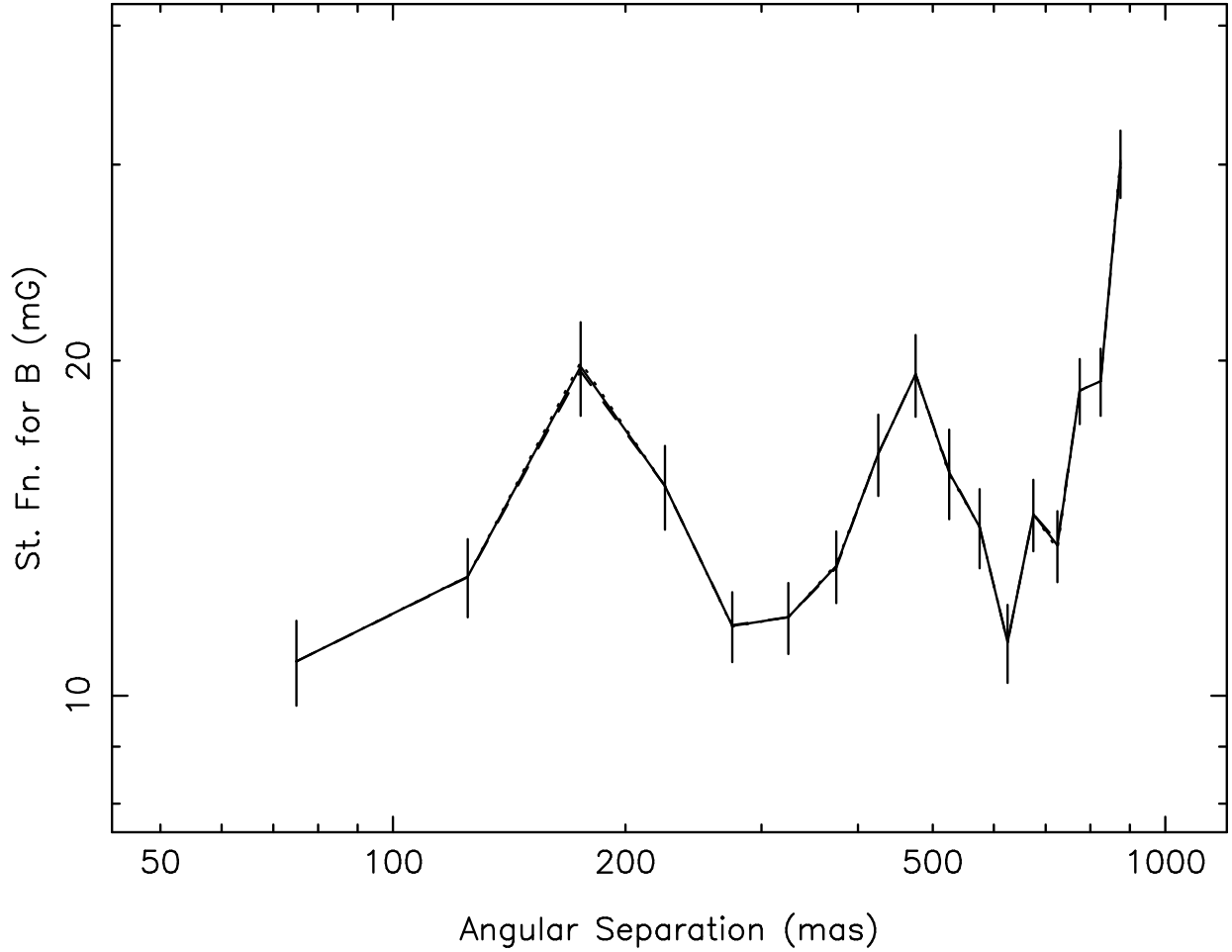


Fig. 8.— Similar to Figure 6, for the magnetic field estimated for the Zeeman pairs. The structure function is in units of  $(\text{mG})^2$ . The strength of the magnetic field within the W49N region seems to show variations on angular scales of 100 mas and beyond. Owing to poor statistics, this structure function estimate is sensitive to binning across the angular separation. See main text for details.